



Multi-Parameter Optimization and Analysis on Performance of a Mixed Flow Pump

X. F. Wu¹, X. Tian^{2†}, M. G. Tan^{2,3} and H. L. Liu^{2,3}

¹ School of Energy and Power Engineering, Jiangsu University, Zhenjiang, Jiangsu, 212013, China

² Research Center of Fluid Machinery Engineering and Technology, Jiangsu University, Zhenjiang, Jiangsu, 212013, China

³ Institute of Fluid Engineering Equipment, Zhenjiang, Jiangsu, 212013, China

†Corresponding Author Email: tianxiao1128@163.com

(Received January 25, 2019; accepted April 27, 2019)

ABSTRACT

A mixed flow pump with guide vanes was chosen as research model in this study, and eight parameters of the impeller were selected as optimization variables, including blade outlet inclination angle, blade wrap angle at hub, blade inlet angle and outlet angle at middle stream line, blade outlet width, front shroud inclination angle, hub inclination angle and vane number. Firstly, orthogonal experimental method and CFD numerical simulation method were used to produce samples, then the RBF neural network was adopted to establish the performance prediction model as the objective function, multi-island genetic algorithm was used for solving the objective function at last. Based on all the above, a method of multi-parameter optimization method on energy performance of mixed flow pump without changing the nominal diameter of impeller outlet was proposed and then verified by experiments. By this method, the pump head and efficiency at the design point of the model pump were increased by 11.5% and 4.32%, respectively. Meanwhile, the peak value of pressure pulsation coefficient at pump inlet, impeller outlet, guide vane outlet and pump outlet all decreased obviously, by a maximum decrease of 62.9%. Compared to the original model, the static pressure in the optimization model increased by 30kPa and the gradient of static pressure distribution after optimization becomes larger and more uniform. The turbulent energy intensity at the impeller outlet was reduced by $0.2\text{m}^2/\text{s}^2$. The pressures at the 60% blade position and 80% blade position both increased by nearly 65kPa and the pressure decreased by 50kPa at the blade pressure side.

Keywords: Energy characteristics; Mixed flow pump; Multi-island GA; Optimization design.

NOMENCLATURE

D_1	impeller inlet diameter	z_1	impeller blade number
D_2	impeller outlet diameter	z_2	diffuser blade number
H	head		
l	impeller outlet width	β_1	installing angle of blade inlet
n	pump rotation speed	β_2	installing angle of blade outlet
n_s	pump specific speed	η	pump efficiency
Q_d	flow rate	θ	blade outlet inclination angle
T_1	front shroud inclination angle	φ	blade hub wrap angle
T_2	hub inclination angle		

1. INTRODUCTION

With the rapid development of economy, the application of mixed flow pump has gradually expanded in China, which plays an important role in

hydraulic engineering. Therefore, to improve efficiency of the mixed flow pump is meaningful for energy saving.

In order to reduce the loss in the guide vane, Jin-Hyu *et al.* (2011) optimized a mixed flow pump with high

specific speed by numerical simulation and the efficiency at design point increased by 7.05%. Heo *et al.* (2016) used response surface method to improve performance of a mixed flow pump and made the efficiency increase by about 1.36% under the regulation flow rate.

Min *et al.* (2015) studied the influence of blade thickness on the performance of the mixed flow pump and found that the efficiency would increase with the decrease of blade thickness. Bing *et al.* (2012), Wu *et al.* (2005) and Zhang *et al.* (2006) simulated the 3D turbulent flow field in a mixed flow pump by CFD and found that the unreasonable design would result in uniform flow, which can deteriorate the performance of pump. Guang *et al.* (2004) and Lu *et al.* (2004) combined CFD simulation with RBF neural network to optimize the performance of a mixed flow pump and succeeded increasing its efficiency from 88.1% to 88.8%. Ruofu *et al.* (2014) applied CFD numerical simulation and orthogonal test method to enlarge the efficiency of the mix-flow pump and make hydraulic efficiency improved by 3.2% under the optimal condition. Zhang *et al.* (2014) optimized the performance of a mixed flow pump by overall consideration of numerical simulation and experimental texts. Li *et al.* (2015) studied the effect of blade tip clearance on the pump performance and found that the larger blade tip clearance can help to reduce the pressure pulsation at impeller inlet area under the small flow conditions, which makes the mixed flow pump run more stably. Duraisamy *et al.* (2019) advocated that by exploiting foundational knowledge in turbulence modeling and physical constraints, data-driven approaches can yield useful predictive models. Ling *et al.* (2016) and Ling *et al.* (2015) established a machine evaluation algorithm and presented a method of using deep neural networks to learn a model for the Reynolds stress anisotropy tensor from high-fidelity simulation data which was more accuracy compared with generic neural network architecture. Ma *et al.* (2015) used Neural Networks (NNs) numerical simulations of bubbly multiphase flows to find closure terms for a simple model of the average flow. The resulting model predicts the evolution of the various initial conditions reasonably well. Derakhshan *et al.* (2013) redesigned impeller by CFD based on optimization algorithm. The results show that the efficiency of centrifugal pump was improved by 3.60%. Bellary *et al.* (2014) optimized the main parameters of impeller by CFD using multi-objective optimization algorithm. The results show that the optimized head is 9.5m and the efficiency is increased by 2.4%. Susanne *et al.* (2005) simplified the model control parameters. The optimization design of the pump blade was completed through parameter cycle iteration by CFD.

Generally, only the key parameters of impellers were selected for optimization of mixed flow pump, whose number was usually less than 5. Meanwhile, the diameter of impeller outlet was usually considered as an optimization variable. However, in order to reduce engineering cost in practical application, it was often requested that the

performance of mixed flow pumps should be improved without changing the diameter of impeller. Based on all above consideration, a new multi-parameter optimization method on improving energy performance of mixed flow pump without changing impeller outlet diameter was proposed in this paper, which was verified by experiments.

2. RESEARCH MODEL

The mixed flow pump with specific speed of 336 was used as the research object. The main design parameters of the pump include flow rate $Q_d=1300\text{m}^3/\text{h}$, head $H=20\text{m}$, rotation speed $n=1450\text{r}/\text{min}$, efficiency $\eta=85\%$, and other main structure parameters were shown in Table 1.

The model pump consists of impellers, guide vanes and discharge elbow. Besides, the impellers and diffusers were all made by casting as shown in Fig. 1.

Table 1 Main structure parameters of model pump

Number	Name	Parameter	Size
1	Inlet diameter/mm	D_1	270
2	Outlet diameter/mm	D_2	320
3	Impeller blade number	z_1	5
4	Impeller outlet width/mm	l	94
5	Blade hub wrap angle / °	φ	110
6	Installing angle of blade inlet / °	β_1	20
7	Installing angle of blade outlet / °	β_2	18
8	Hub inclination angle / °	T_2	48
9	Front shroud inclination angle / °	T_1	40
10	Blade outlet inclination angle / °	θ	34
11	Diffuser blade number	z_2	7

3. TEST OF ENERGY PERFORMANCE

Figure 2 shows the test performance curves of the model pump. As shown in Fig. 2, the pump efficiency is 81.08% and the head is 18.10m at the design point. Compared with design requirements, the efficiency is lower by 3.92%, and the head is lower by 1.9m. Besides, with the increase of flow rate, the head decreases fast. The efficiency curve is rather flat under large flow rate. The pump efficiency maintains upper 80% when the flow rate is between $1200\text{m}^3/\text{h}$ and $1350\text{m}^3/\text{h}$, which can be defined as high efficiency area. So, the high efficiency span of

this pump is only 150m³/h.

According to the test results, it is necessary to optimize the mixed flow pump to meet the design requirements.



(a) impeller



(b) guide vanes

Fig. 1. The mixed-flow pump model.

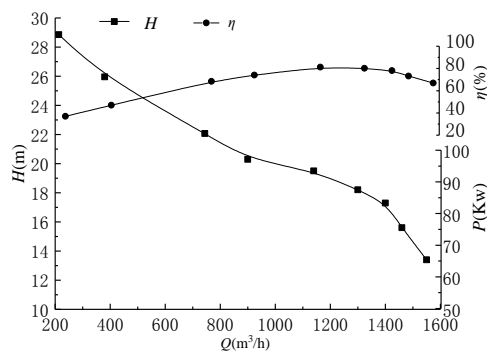


Fig. 2. Performance curves of the model pump.

4. NUMERICAL CALCULATION OF MODEL PUMP

In order to predict the performance of following optimization samples by CFD accurately, the internal flow simulation method of the model pump was discussed at first step.

4.1 3D Model and Grid Generation

As shown in Fig. 3, the calculation domain consists

of inlet extension, impeller, clearance between impeller and diffuser, diffuser, discharge elbow and outlet extension. In order to simulate the rotational effect, the multiple frames of reference were involved. The impeller was set to be the rotational, and the remaining flow field was set to be the stationary. ICEM15.0 was used to generate the grid of computational domain and all computational domains were generated into hexahedral cells to improve simulation precision. The grid of computing domain was shown in Fig. 3.

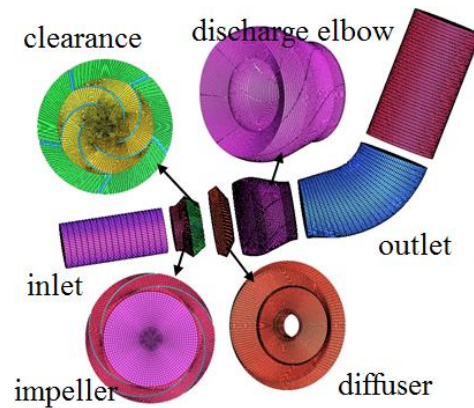


Fig. 3. Grid of computational domain.

4.2 Grid Independence Check

The accuracy of simulation results increases with the number of the total grid. A grid independence check was carried out, including four schemes, to eliminate the effects of grid number on the simulation results. The total grid number of four schemes were 1.4million, 2.84million, 3.54million, 5.14million. The head under design flow rate was used as the criteria. The simulation results were shown in Fig. 4. The y^+ value is less than 40 and it satisfies the requirements of turbulence model. It can be seen that when the total grid number is less than the 3.5 million, the calculated head increases with the total grid number. Head difference between 3.5 million total grid number and 5.1 million total grid number is just 0.01 m, only about 0.06 percent when the flow rate is 1300 m³/h. Therefore, considering the calculation resource and time, the 3.5 million total grid number was selected finally.

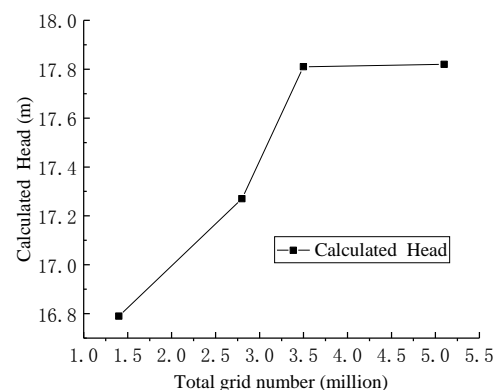


Fig. 4. Grid independency check.

4.3 Numerical Method

CFX15.0 was used to conduct steady numerical simulation of the pump internal flow; the turbulence was modeled by SST turbulence model. Besides, five operating points of $0.8Q_d$, $0.9Q_d$, $1.0Q_d$, $1.1Q_d$ and $1.2Q_d$ were considered.

The inlet boundary condition of computing domain was set as pressure inlet by 1 atm, and the outlet boundary condition was set as the mass flow outlet; in calculation, the PRESTO format was used to discrete pressure term, the second order windward format was used to discrete convection terms, and the others are discrete by second order center difference scheme. Also, the non-slip wall surface was adopted, and the roughness was set to be 0.05mm. Frozen rotor interface was used for constant calculation.

4.4 Validation of the Method

The comparison between experimental test and numerical prediction of the model pump external characteristics is shown in Fig. 5. As can be seen, the head and efficiency curve of the numerical calculation is basically consistent with the trend of the test. The head decreases with the increase of the flow rate, and the efficiency increases first and then decreases with the increase of the flow rate, and the calculated value of the head is slightly lower than the experimental value. At the small flow rate, the calculation value of efficiency is slightly lower than that of experiment, but the calculation value of efficiency is slightly higher than the experimental value under big flow rate.

Quantitative analysis shows that the CFD prediction value of efficiency is 80.848% while the test value is 81.08%, the distance is only 0.232%. The CFD prediction value of head is 17.81m while the test value is 18.1m, and the predicted deviation is 1.6%. Pump test efficiency and efficiency of CFD are very closed to each other, which is due to that the efficiency of CFD is modified by empirical formula to include the volumetric efficiency and mechanical efficiency. The errors between calculation results and test results are all within 3% at each condition, which shows that CFD numerical calculation method is enough accurate and it can be used for subsequent performance prediction of sample points.

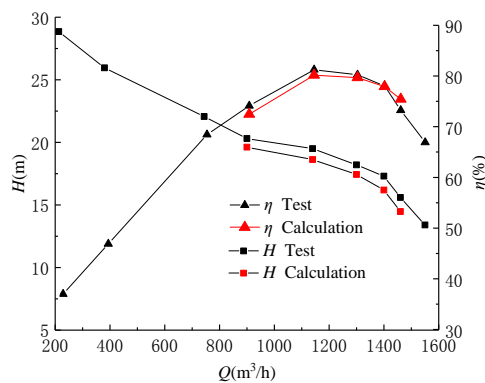


Fig. 5. Test and numerical simulation curves.

5. MULTI-PARAMETER OPTIMIZATION

5.1 Establishment of Sample Points

Eight parameters of impeller, such as blade outlet edge inclination angle θ , blade wrapping angle at hub φ , inlet angle β_1 and outlet angle β_2 at blade middle streamline, blade outlet width l , front shroud inclination angle T_1 , hub inclination angle T_2 and vane number z were selected to do optimization.

Table 2 Factor level table

Factor	Level 1	Level 2	Level 3	Level 4
$\varphi(^{\circ})$	90	96.7	103.3	110
$T_1(^{\circ})$	28	32	36	40
$\beta_1(^{\circ})$	12	15.3	18.7	22
$\beta_2(^{\circ})$	18	21.3	24.7	28
$T_2(^{\circ})$	50	55	60	65
$\theta(^{\circ})$	22	28	34	40
l (mm)	84	91	97	104
z	4	5		

Orthogonal test was helpful for balancing the test factors and the distribution of data points, which can greatly reduce the number of test. Therefore, based on orthogonal test and CFD numerical calculation, blade number was set to be 2 levels, the other 7 optimization variables were set to be 4 levels to obtain sample points. The factor level table is shown in Table 2.

64 sets of research schemes were obtained by L64 mixed orthogonal table design. Because of project quantity, to save the calculation resources, Isight 5.5 was chosen to be the optimization platform, which can integrate 3d modeling software ProE, mesh generation software ICEM and numerical calculation software CFX.

5.2 Orthogonal Test Results

Due to limited space, only 10 sample data was listed here, as shown in Table 3.

5.3 Establishment of Performance Prediction Model

Compared with other neural networks, RBF neural network has the advantages of high efficiency, simple structure, fast training speed, good approximation performance and global optimization.

RBF neural network was used to predict the performance of mixed flow pump to provide goal function for the next performance optimization of mixed flow pump. Based on RBF neural network, the performance of mixed flow pump was predicted by building the relation between input parameters (8 optimization parameters) and to output parameters (head, efficiency).

Table 3 Orthogonal test scheme

Number	θ	l	β_1	Φ	β_2	T_1	T_2	z	$H(m)$	$\eta(\%)$
1	1	1	1	1	1	1	1	1	16.83	84.23
2	1	1	1	4	2	2	2	1	15.17	81.65
3	1	1	4	1	2	2	2	1	16.71	82.75
4	1	1	4	4	1	1	1	1	13.81	83.73
5	1	2	1	2	3	3	3	1	18.58	82.15
6	1	2	1	3	4	4	4	1	18.45	78.47
7	1	2	4	2	4	4	4	1	18.46	81.06
8	1	2	4	3	3	3	3	1	17.09	82.25
9	1	3	2	2	2	4	4	2	20.71	82.58
10	1	3	2	3	1	3	3	2	19.34	84.35

Based on the samples obtained by orthogonal experiments, 1~60 sets of data were selected to train RBF neural network prediction model, and 61~64 groups were used as test samples. Figure 6 shows the mean square error variation curve of the RBF neural network. As can be seen from Fig. 6 the network completes the training in 300 steps, while the learning error accuracy gets lower than 10^{-3} .

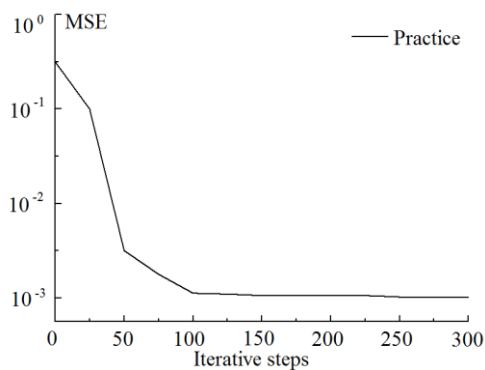


Fig. 6. RBF mean square error variation curve of neural network.

According to the error analysis, the multiple correlation coefficients of the head and efficiency generated by the neural network are 0.928 and 0.912 respectively. The correlation coefficients are all above 0.9, which means that the approximation model has good precision.

5.4 Optimization Algorithm

Multi-island genetic algorithm was used to solve the performance prediction model. Figure 7 shows the optimization process based on the multi-island

genetic algorithm.

The optimization purpose was to improve the efficiency of the mixed flow pump while the head requirement must be met. So, the constraint was that $H \geq 20m$ and $85\% \leq \eta\% \leq 100\%$. The ranges of optimization variables were that $18 \leq \beta_2 \leq 28$, $50 \leq T_2 \leq 65$, $84 \leq l \leq 104$, $22 \leq \theta \leq 40$, $90 \leq \varphi \leq 110$, $28 \leq T_1 \leq 40$, $12 \leq \beta_1 \leq 22$, $z = 4, 5$.

There were 1002 steps in the optimization of the total iteration. From the 400th steps, the obvious local convergence appears. As optimization calculation goes on, the number of local convergence gradually increases and the convergence situation was good. Finally, all the iterative computation data were arranged to obtain global search results.

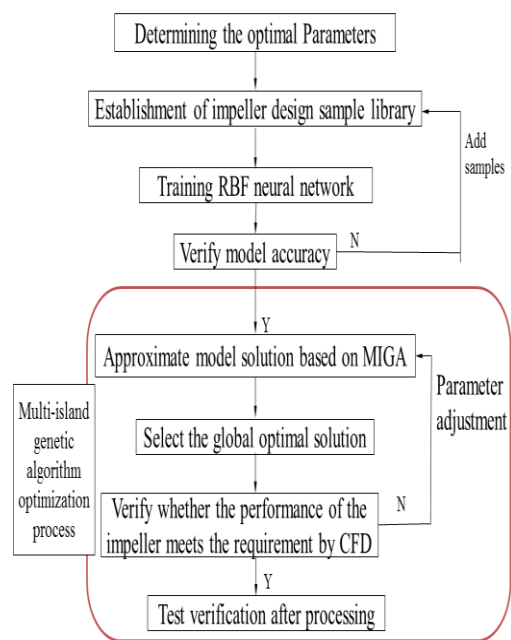
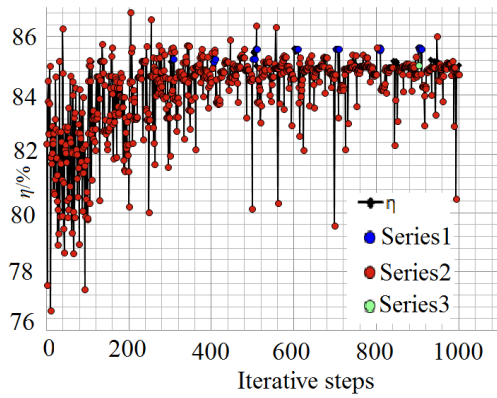


Fig. 7. Optimization process of multi Island genetic algorithm.

Figure 8 is the distribution of efficiency and head during the optimization procedure. In Fig. 8, the blue point represents the feasible solution, which can satisfy the constraint conditions. The red point represents unfeasible solution, which cannot satisfy the constraint condition. The green point represents the optimal solution. Therefore, the global optimal solution was that $\eta=85\%$ and $H=20.6m$.

5.5 Optimization Results

As shown in Table 4, after optimization, the blade number was 4, and the blade outlet edge inclination angle θ , blade wrapping angle at hub φ , blade outlet angle β_2 and front shroud inclination angle T_1 got smaller, which were reduced by 10.3%, 8.6%, 10% and 18.3% respectively. The blade outlet width l , blade inlet angle β_1 at middle streamline and hub inclination angle T_2 became bigger, which were increased by 6.4%, 1.5% and 14.6% respectively.



(a) efficiency

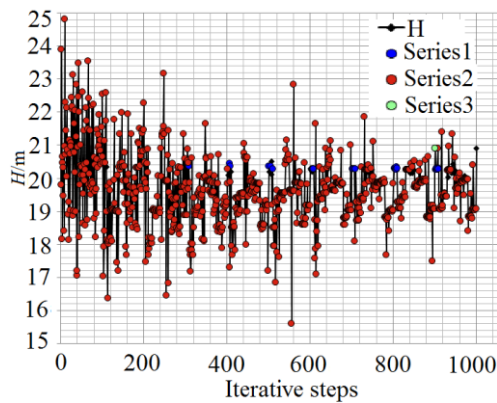


Fig. 8. Distribution of efficiency and head during the optimization progress.

Table 4 Comparison of parameters before and after optimization

Variable	Before optimization	After optimization
$\theta(^{\circ})$	34	30.5
l (mm)	94	100
$\beta_1(^{\circ})$	20	20.3
$\varphi(^{\circ})$	110	100.5
$\beta_2(^{\circ})$	20	18
$T_1(^{\circ})$	40	32.7
$T_2(^{\circ})$	48	55
Z	5	4

6 COMPARISON OF THE PERFORMANCE OF MODEL PUMP BEFORE AND AFTER OPTIMIZATION

In order to verify the optimization results, the optimized impeller was manufactured and tested. Figure 9 presents the new impeller.

6.1 Energy Performance

The energy performance comparison between the

optimized model and the original model is shown in Fig. 10. As shown in Fig. 10, the optimized head curve is basically the same as before optimization, but its slope gets smaller at large flow rate. Under small flow rate, the optimized efficiency curve is slightly higher than that before optimization, but the trend of variation is basically the same. Under large flow rate, the optimized efficiency curve is obviously more flat.

After optimization, the maximum efficiency was at $1348\text{m}^3/\text{h}$ and the efficiency was 86.08%, the head was 19.98m. Compared with the original model pump, the efficiency has increased by 5 % and the head has increased by 10.38%. At the design point ($Q_d=1300\text{m}^3/\text{h}$), the head and efficiency of the optimized pump were 20.18m and 85.4%, which had increased by 11.5% and 4.32% respectively. Therefore, the optimization was successful and can meet the design requirements.



Fig. 9. Optimized impeller.

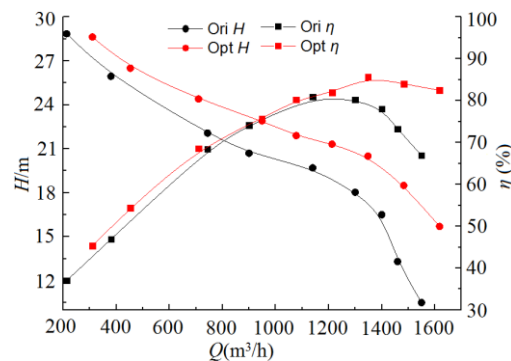


Fig. 10. Comparison of performance curves before and after optimization.

From Fig. 10, it can be found that the efficiency of optimized pump was always higher than 80% between $1000\text{m}^3/\text{h}$ and $1550\text{m}^3/\text{h}$. Therefore, the high efficiency area span increased to $550\text{m}^3/\text{h}$, which is 3.67 times bigger than that before optimization.

That is to say, the overall performance of this pump becomes improved, and the range of the high efficiency range is widened.

6.2 Pressure Pulsation

In order to compare the pressure pulsation

performance between the original model and optimized pump, four monitoring points were arranged, as shown in Fig. 11. P1 was at pump inlet, P2 was at guide vane inlet, P3 was at guide vane outlet and P4 was at pump outlet.

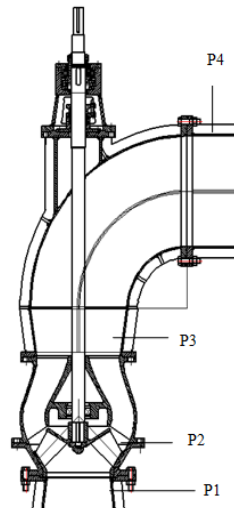


Fig. 11. Monitoring points of pressure pulsation.

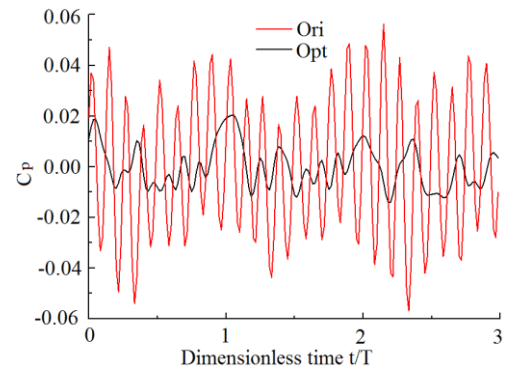
Figure 12 presents the pressure pulsation in time domain at $1.0Q_d$. As can be seen, the pressure pulsation curves at each monitoring point all show a certain periodicity. From the P1 point to the P4 point, the pressure pulsation coefficient first increases and then decreases, and pressure pulsation at P2 is the maximum, the pressure pulsation at P4 is the minimum. Besides, the peak value of the pressure pulsation coefficient at P2 is 4.77 times bigger than that at the P4. The amplitude of the pressure pulsation at the P3 is the maximum after optimization, indicating that the pressure pulsation is severest here under the $1.0Q_d$ condition. The peak value of pressure pulsation of P1, P2, P3 and P4 gets reduced by 62.9%, 37.5%, 28.57% and 62.5%, respectively after optimization, which means that the pressure pulsation condition gets improved.

6.3 Internal Flow Field

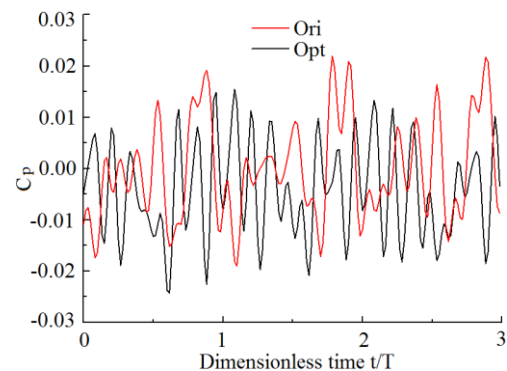
As known, the internal flow determines the performance for fluid machinery. In order to find out the mechanism how the performance got improved, the inner flow in this mixed flow pump was compared and analyzed in details before and after optimization.

Figure 13 shows the static pressure distribution in axial middle section of impeller before and after optimization under $1.0Q_d$ condition. Obviously, two pictures all show the similar pressure distribution. The inlet lower pressure area is in two sides of the impeller inlet while higher pressure area is in the middle of the impeller inlet. Meanwhile, the pressure increases from impeller inlet to outlet gradually. But the gradient of static pressure distribution after optimization becomes larger and more uniform and the pressure at outlet gets larger. Compared to the original model, the static pressure in the optimization model increased by 30kPa. This is mainly because

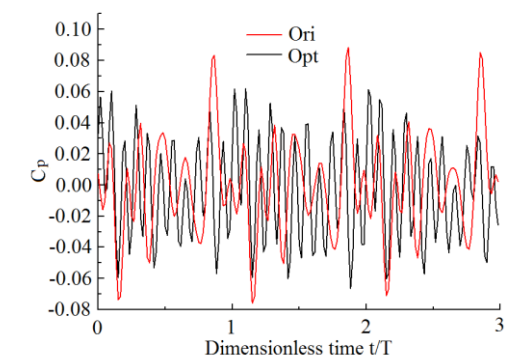
the flow in the optimized impeller was improved and gets more uniform, which makes the inlet impact loss decrease. So the low pressure area at the impeller inlet was reduced.



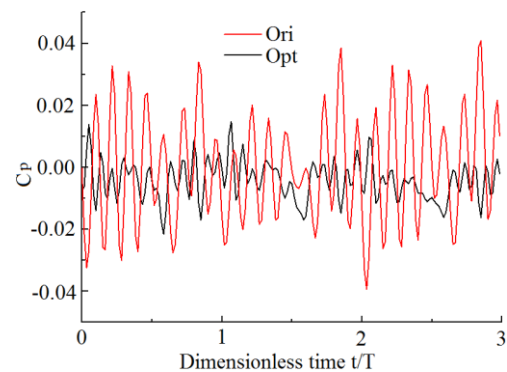
(a) P1



(b) P2



(c) P3



(d) P4

Fig. 12. Pressure pulsation in time domain at $1.0Q_d$.

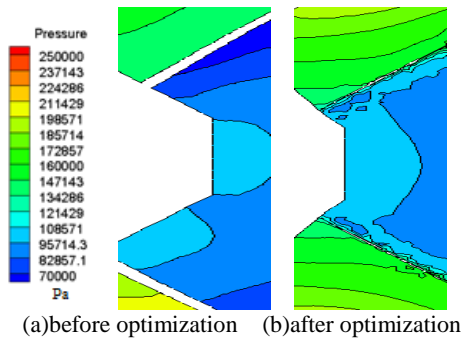


Fig. 13. Static pressure distribution in axial middle section of impeller under $1.0Q_d$.

Figure 14 shows the distribution of turbulent kinetic energy in axial middle section of impeller before and after optimization under $1.0Q_d$. As can be seen from Fig. 14, the maximum turbulent kinetic energy before optimization is near the rim in whole impeller, which indicates most unstable flow is here and great energy loss. Further comparison shows that the turbulent kinetic energy intensity at the rim decreases after optimization, which means that the flow gets more stable and the flow loss is reduced. So the pump efficiency is improved.

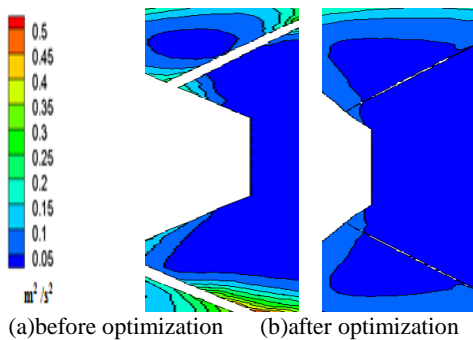
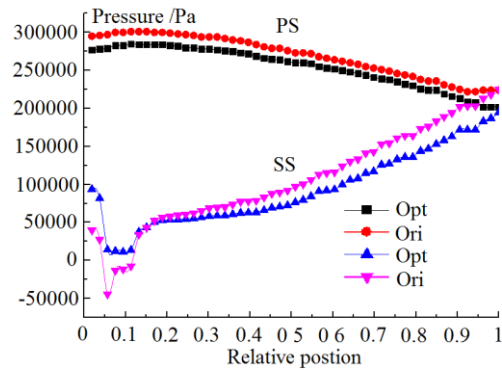


Fig. 14. Distribution of turbulent kinetic energy in axial middle section of impeller under $1.0Q_d$

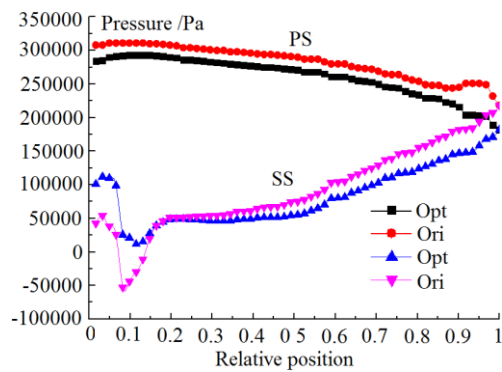
Figure 15 shows static pressure distribution before and after the optimization at the 60% and 80% blade height positions under $1.0Q_d$. In Fig. 15, 0-1 represents the position along the blade surface, 0 represents the blade inlet and 1 represents the blade outlet. The PS represents the blade pressure side and the SS represents the blade suction side.

As shown in Fig. 15, the changing tendency of static pressure distribution along radius direction at the 60% and 80% blade height positions is almost the same. The static pressure at the blade pressure side gradually decreases from the blade inlet to the outlet, while the static pressure at the blade suction side increases gradually from blade inlet to outlet. Besides, there exists a "concave" near the inlet at the suction side, which means that there appears a pressure drop here and the vortex is more likely to appear.

By further comparison, it can be seen that the pressures at blade pressure side of the two curves all decrease and the drop amplitude all is about 50 kPa at the inlet.



(a) 60% blade height



(b) 80% blade height

Fig. 15. Static pressure distribution before and after the optimization under $1.0Q_d$.

From 0 to 0.1, the pressures at blade suction side of two curves are all increased by nearly 65 kPa. But the pressure at blade suction side from 0.2 to 1 is decreased a little. This variation means the optimization reduce the pressure difference at inlet and make the pressure of suction side at inlet bigger. Therefore, the unstable flow at inlet caused by pressure difference can be effectively suppressed.

7. CONCLUSION

A multi-parameter optimization method for mixed-flow pump performance without changing the nominal diameter of impeller outlet is proposed in this paper.

- (1) Eight parameters of impeller, including blade outlet inclination angle, blade wrap angle at hub, blade inlet angle and outlet angle at middle stream line, blade outlet width, front shroud inclination angle, hub inclination angle and vane number, were selected to optimize the performance of the pump. RBF neural network model was used to establish the performance prediction model of mixed-flow pump. The sample points of training and testing were determined by orthogonal test and CFD numerical simulation. The genetic algorithm was used to solve the prediction model. The numerical results showed that the performance of the model pump has been significantly improved after optimization.

- (2) At designed point, the head and efficiency of the optimized pump were 20.18m and 85.4%, which had increased by 11.5% and 4.32 percentages respectively and the high efficiency area got 3.67 times bigger after optimization. Besides, the peak value of pressure fluctuation decreased by 62.9%.
- (3) The internal flow became more stable since the static pressure got uniform and the turbulent kinetic energy intensity decreased. The static pressure in the optimization model increased by 30kPa. The turbulent energy intensity at the impeller outlet was reduced by $0.2\text{m}^2/\text{s}^2$. The pressures at the 60% blade position and 80% blade position both increased by nearly 65kPa. The pressure decreased by 50kPa at the blade pressure side. All of these make the overall performance of pump greatly improved.

ACKNOWLEDGEMENTS

The authors gratefully acknowledge the support of the following foundations:

The National Natural Science Foundation of China, Grant 51509109, 51679110 and 51779108.

The Foundation of Jiangsu Province, Grant BK20161350, BE2017356;

The Priority Academic Program Development of Jiangsu Higher Education Institutions (PAPD).

REFERENCES

- Bellary, S. A. I., A. Husain and A. Samad, A. (2014). Effectiveness of meta-models for multi-objective optimization of centrifugal impeller. *Journal of Mechanical Science and Technology*, 28(12), 947-957.
- Bing, H., S. Cao, L. Tan and L. Lu (2012). Effects of diffuser vane on mixed-flow pumps performance. *Journal of Drainage & Irrigation Machinery Engineering* 30(2), 125-130.
- Derakhshan, S., M. Pourmahdavi, E. Abdollahnejad, A. Reihani and A. Ojaghi (2013). Numerical shape optimization of a centrifugal pump impeller using artificial bee colony algorithm. *Computers & Fluids* 81, 145-151.
- Duraisamy, K., G. Iaccarino and H. Xiao (2019). Turbulence modeling in the age of data. *Annual Review of Fluid Mechanics* 51, 1-23.
- Guang, X. I., L. U. Jinling and Q. I. Datong (2004). Research on the optimization method of 3-d blade in mixed-flow pump. *Journal of Engineering Thermophysics* 25(6), 952-955.
- Heo, M. W., K. Y. Kim, J. H. Kim and Y. S. Choi (2016). High-efficiency design of a mixed-flow pump using a surrogate model. *Journal of Mechanical Science and Technology* 30(2), 541-547.
- Jin-Hyu, K. and K. Kwang-Yong, (2011). Optimization of vane diffuser in a mix-flow pump for high efficiency design. *International Journal of Fluid Machinery System* 4(1), 72-178.
- Li, R. N., P. L. Hu, Y. B. Li, Z., Bi and D. Zhou (2015). Numerical analysis of effect of blade tip clearance on pressure fluctuation in mixed-flow pump inlet. *Journal of Drainage & Irrigation Machinery Engineering* 33(07), 560-565.
- Ling, J. and J. Templeton (2015). Evaluation of machine learning algorithms for prediction of regions of high Reynolds averaged Navier Stokes uncertainty. *Physics of Fluids* 27(8), 085103.
- Ling, J., A. Kurzwski, and J. Templeton (2016). Reynolds averaged turbulence modelling using deep neural networks with embedded invariance. *Journal of Fluid Mechanics* 807, 155-166.
- Lu, J., G. Xi and D. Qi (2004). Blade optimization of mixed-flow pump by using inverse design method and neural network. *Journal of Xian Jiaotong University* 38, 308-314.
- Ma, M., J. Lu and G. Tryggvason (2015). Using statistical learning to close two-fluid multiphase flow equations for a simple bubbly system. *Physics of Fluids* 27(9), 092101.
- Min, G., Y., L. U. Sheng, G. Bo, W. Da, W. Jun and J. University (2015). Influence of blade thickness on energy performance of mixed flow nuclear main pump. *Fluid Machinery* 5, 28-32.
- Ruofu, X., T. Ran, W. Weiwei and Y. Wei (2014). Inverse design and hydraulic optimization of mixed-flow pump impeller. *Transactions of the Chinese Society for Agricultural Machinery* 45(9), 84-88.
- Susanne, T. and S. Rudolf (2005). Optimization of hydraulic machinery bladings by multilevel CFD techniques. *International Journal of Rotating Machinery* 2, 161-167.
- Wu, Z. and W. Zhao (2005). Numerical simulation of interior flow field of mixed flow Pump. *Fluid Machinery* 10, 15-19.
- Zhang, D. S., W. D. Shi, D. Z. Pan, W. D. Cao and T. T. Li (2014). Hydraulic performance optimization and experiment of special mixed-flow pump based on numerical simulation. *Journal of Mechanical Engineering* 50(6), 177-184.
- Zhang, X. Y., G. Y. Wang, Z. Y. Yu and Z. Z. Han (2006). Performance improvement of a mixed flow pump stage based on CFD. *Journal of Engineering Thermophysics* 27(5), 772-777.

APPENDIX

Orthogonal test scheme

Number	θ	l	β_1	Φ	β_2	T_1	T_2	z	$H(m)$	$H(\%)$
1	1	1	1	1	1	1	1	1	16.83	84.23
2	1	1	1	4	2	2	2	1	15.17	81.65
3	1	1	4	1	2	2	2	1	16.71	82.75
4	1	1	4	4	1	1	1	1	13.81	83.73
5	1	2	1	2	3	3	3	1	18.58	82.15
6	1	2	1	3	4	4	4	1	18.45	78.47
7	1	2	4	2	4	4	4	1	18.46	81.06
8	1	2	4	3	3	3	3	1	17.09	82.25
9	1	3	2	2	2	4	4	2	20.71	82.58
10	1	3	2	3	1	3	3	2	19.34	84.35
11	1	3	3	2	1	3	3	2	19.84	83.93
12	1	3	3	3	2	4	4	2	20.97	82.65
13	1	4	2	1	4	2	2	2	23.94	79.92
14	1	4	2	4	3	1	1	2	21.04	81.26
15	1	4	3	1	3	1	1	2	23.07	80.54
16	1	4	3	4	4	2	2	2	21.41	78.13
17	2	1	2	1	3	3	4	1	19.03	81.04
18	2	1	2	4	4	4	3	1	16.84	78.71
19	2	1	3	1	4	4	3	1	18.87	81.44
20	2	1	3	4	3	3	4	1	16.50	78.92
21	2	2	2	2	1	1	2	1	18.26	83.41
22	2	2	2	3	2	2	1	1	17.60	85.30
23	2	2	3	2	2	2	1	1	18.10	84.49
24	2	2	3	3	1	1	2	1	17.26	84.76
25	2	3	1	2	4	2	1	2	22.82	80.79
26	2	3	1	3	3	1	2	2	21.97	81.45
27	2	3	4	2	3	1	2	2	21.99	81.71
28	2	3	4	3	4	2	1	2	21.32	83.01
29	2	4	1	1	2	4	3	2	23.63	80.29
30	2	4	1	4	1	3	4	2	21.26	80.94
31	2	4	4	1	1	3	4	2	22.80	77.91
32	2	4	4	4	2	4	3	2	20.61	82.40
33	3	1	2	2	3	2	3	2	21.07	82.15
34	3	1	2	3	4	1	4	2	21.44	79.65
35	3	1	3	2	4	1	4	2	21.95	80.85
36	3	1	3	3	3	2	3	2	20.07	82.33
37	3	2	2	1	1	4	1	2	20.83	82.79
38	3	2	2	4	2	3	2	2	19.67	82.46
39	3	2	3	1	2	3	2	2	21.70	81.12
40	3	2	3	4	1	4	1	2	18.30	85.32
41	3	3	1	1	4	3	2	1	22.61	79.46
42	3	3	1	4	3	4	1	1	19.20	81.83
43	3	3	4	1	3	4	1	1	20.74	81.03
44	3	3	4	4	4	3	2	1	19.59	81.52
45	3	4	1	2	2	1	4	1	22.90	78.65
46	3	4	1	3	1	2	3	1	21.03	81.70
47	3	4	4	2	1	2	3	1	21.04	79.50
48	3	4	4	3	2	1	4	1	21.41	80.29
49	4	1	1	2	1	4	2	2	20.23	84.36
50	4	1	1	3	2	3	1	2	20.08	82.87
51	4	1	4	2	2	3	1	2	20.09	84.57

Number	θ	l	β_1	Φ	β_2	T_1	T_2	z	$H(m)$	$H(\%)$
52	4	1	4	3	1	4	2	2	18.74	84.98
53	4	2	1	1	3	2	4	2	24.52	78.63
54	4	2	1	4	4	1	3	2	22.84	77.07
55	4	2	4	1	4	1	3	2	24.38	77.02
56	4	2	4	4	3	2	4	2	21.50	80.81
57	4	3	2	1	2	1	3	1	22.82	76.05
58	4	3	2	4	1	2	4	1	19.94	83.36
59	4	3	3	1	1	2	4	1	21.97	77.17
60	4	3	3	4	2	1	3	1	20.28	82.13
61	4	4	2	2	4	3	1	1	23.51	78.41
62	4	4	2	3	3	4	2	1	22.16	80.71
63	4	4	3	2	3	4	2	1	22.67	80.11
64	4	4	3	3	4	3	1	1	22.51	79.38

K_1 , K_2 , K_3 and K_4 represent four levels of factors respectively. The influence weight of each parameter on efficiency can be determined by the range R of each parameter. The weight of parameters increased with the R value. Therefore, ranking R can determine the influence degree of eight optimization parameters on efficiency.

Effect of Optimizing Parameters on Efficiency

	K_1	K_2	K_3	K_4	R	Rank
$\theta(^{\circ})$	81.86	81.67	81.29	80.48	1.38	5
$L(mm)$	80.17	82.14	81.7	81.36	1.97	4
$\beta_1(^{\circ})$	80.91	81.39	81.46	81.54	0.62	7
$\varphi(^{\circ})$	82.14	81.27	80.09	81.8	2.05	3
$\beta_2(^{\circ})$	82.66	81.9	81.06	79.69	2.97	1
$T_1(^{\circ})$	80.8	81.36	81.33	81.8	1	6
$T_2(^{\circ})$	82.48	81.79	80.85	80.19	2.28	2
z	81.12	81.53			0.41	8